(5) V. T. Lam, P. Picker, D. Patterson, and P. Tancrede, *J. Chem. Soc., Faraday Trans. 2*, **70**, 1476 (1974).
(6) A. Weissberger, "Technique of Organic Chemistry", Vol. VII, Interscience, New York, N.Y., 1955.
(7) E. Calvet and H. Prat, "Recent Progress in Microcalorimetry", Pergamon Press, New York, N.Y., 1963.
(8) M. B. Ewing and K. N. Marsh, *J. Chem. Thermodyn.*, **2**, 352 (1970).
(9) S. Murakami and G. C. Benzon, *J. Chem. Thermodyn.*, **1**, 565 (1969).
(10) R. A. Orwoll, P. J. Flory, J. L. Ellenson, and B. E. Eichinger, *Macromolecules*, **1**, 283 (1968).
(11) A. Abe and P. J. Flory, *J. Am. Chem. Soc.*, **87**, 1840 (1965).
(12) P. Tancrede, D. Patterson, and V. T. Lam, *J. Chem. Soc., Faraday Trans. 2*, **71**, 994 (1975).

Neutron Scattering by Uniaxially Hot Stretched Polystyrene Samples

C. Picot,* [1a] R. Duplessix, D. Decker,[1a] H. Benoit,[1a] F. Boue,[1b] J. P. Cotton,[1b] M. Daoud,[1b] B. Farnoux,[1b] G. Jannink,[1b] M. Nierlich,[1b] A. J. de Vries,[1c] and P. Pincus[1d]

C.R.M., 67083 Strasbourg, France; Laboratory Léon Brillouin, CENS, 91120 Gif, sur Yvette, France; Centre de Recherche de la Croix de Berny, Rhône Poulenc Industries, 92160 Antony, France; Collège de France, 75231 Paris, France; and Laboratory de Physique des Solides, Université Paris Sud, 91405 Orsay, France.
Received January 23, 1976

ABSTRACT: Neutron small-angle scattering experiments by tagged polystyrene films hot stretched and subsequently quenched are discussed in terms of coil deformation. The parameters which are varied in this experiment are the extension ratio λ, the hot stretch temperature T_1, and in one case a partial recovery between the stretch and quench phases. The nature of the deformation is examined at different pair correlation distances r, in between R'' the coil size in the stretch direction and l the step length. Below a length r^*, we find deviations to the affine deformation in the longitudinal direction. This deviation increases, at given λ, with the hot stretch temperature and shows how the loss of molecular orientation observed in birefringence is compatible with a total recovery of the sample after annealing.

(I) Uniaxial Stretching

In this report we examine the deformation of coils in uniaxially hot stretched polystyrene films. The samples are films of lengths $L_0 \simeq 3$ cm, made of a mixture of 99% protonated and 1% deuterated polystyrene ($M_w = 1.17 \times 10^5$). The molecular weight dispersion[2a] is $M_w/M_n = 1.1$. At a given temperature T_1 above the glass transition T_G (~95 °C), they are stretched with a velocity gradient $s(t) = (1/L(t))\, dL(t)/dt$, where $L(t)$ is the length of the film at time t. Upon stretching, they are quenched at a temperature $T_2 \ll T_G$ while being maintained at the fixed end-to-end length L. A neutron small-angle scattering measurement is then made at room temperature. One sample, labeled Re, is allowed to relax before quenching by letting the end-to-end length decrease from $\tilde{L}$ to $\tilde{L} = 0.95L$, at the temperature T_1. Only thereafter is it frozen in and measured. The sequence of events is seen in Figure 1. The figure shows in fact the succession of a stretching phase in the time interval $(0,t_1)$ and a quench phase in the interval (t_2,t_3). The time necessary to switch from one phase to the other is $(t_2 - t_1)$ and is kept as small as possible. During the time $(t_3 - t_1)$ the sample is kept at the fixed end-to-end length L at a temperature which decreases from T_1 but is still above T_G. The stress relaxes and therefore (t_1,t_3) will be called a stress relaxation phase. For sample Re, the stress relaxation is preceded by a strain relaxation phase.

Molecular orientation frozen in such samples has been measured by birefringence experiments[2b,3] and was found to be dependent upon the stretch ratio $\lambda = L_0/L$ and the temperature T_1. In particular, for a given λ, birefringence and consequently orientation decrease as T_1 increases. This observation is difficult to interpret, because the samples generally recover their initial length L_0 when annealed at a temperature greater or equal to T_1 after quenching. Thus on the macroscopic scale, the deformation is purely elastic (this was not tested on our samples but is inferred[3] from earlier hot stretch experiments with higher molecular weights). On the microscopic scale, there must on the contrary be a form of viscous deformation since molecular orientation is increasingly relaxed as the temperature is raised. We expect thus that the decomposition of the deformation[2b]

$$\lambda - 1 = \lambda_i + \lambda_{he} + \lambda_v - 3 \qquad (1)$$

into instantaneous, high elastic, and viscous deformations is not identically the same at different spatial scales. On the scale L, the last term is negligible with respect to the second and first terms in our experimental conditions. On the segment scale, the situation is very different. We expect from the scattering experiment to cover part of the intermediate situations because of the possibilitity of exploring reciprocal space by variation of the scattering angle. We can think of two types of coil deformation in the hot stretch phase.

(A) The deformation is *uniformly* affine,[4] which amounts to saying that every vector $\mathbf{r}_{ij} = (x_{ij}, y_{ij}, z_{ij})$ joining two coil segments (i,j) is transformed into $\bar{\mathbf{r}}_{ij} = (\lambda x_{ij}, \lambda^{-1/2} y_{ij}, \lambda^{-1/2} z_{ij})$, the x axis being the uniaxial stretch direction. As a consequence, the average squared orientation of a coil segment with respect to the x axis (molecular orientation) is[5]

$$\langle \cos \omega^2 \rangle = \tfrac{1}{3} + 2(\lambda - 1)/5 + \ldots \qquad (\lambda - 1 \simeq \epsilon) \qquad (2)$$

In this context, the result is of course totally independent of molecular weight.

(B) In another version,[6] which applies to rubber elasticity, the affine deformation theory holds true only for distances separating effective cross links. Let $\mathbf{r}_{pq}$ be such a vector. Then $\bar{\mathbf{r}}_{pq} = (\lambda x_{pq}, \lambda^{-1/2} y_{pq}, \lambda^{-1/2} z_{pq})$, but for all $\mathbf{r}_{ij}$ inside $\mathbf{r}_{pq}$ the deformation of the coil is determined by the response of a brownian chain to the constraint (p,q). As a result, the average

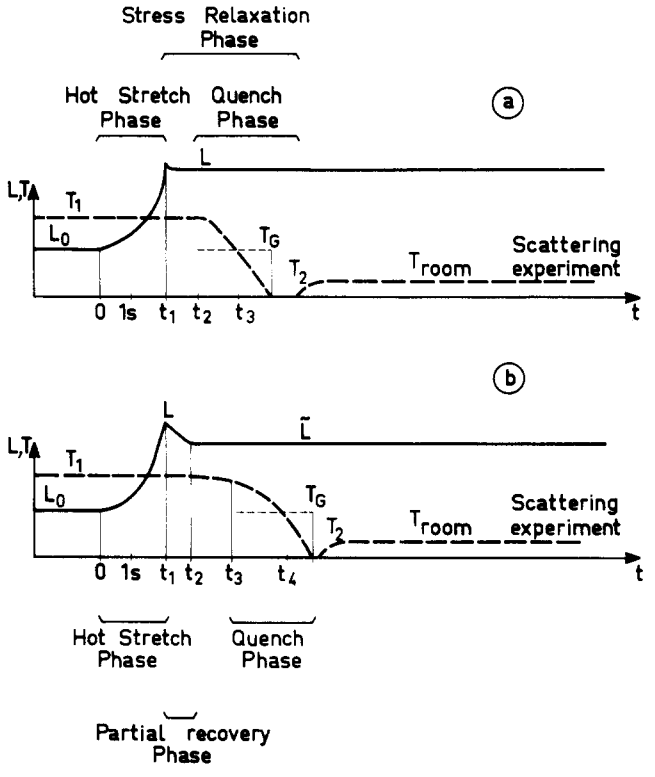

Figure 1. Schematic time sequence for film length L and hot stretch temperature T_1 in the uniaxial extension of the polystyrene films. The time scale is approximative and the variations of L and T_1 are only indicative: (a) normal; (b) with partial recovery in between the stretch and quench phases.

squared orientation[6] of the segments is closer to ⅓ than in hypothesis A.

$$\langle \cos^2 \omega \rangle = \tfrac{1}{3} + 2(\lambda^2 - 1/\lambda)/(15|p - q|) + \dots \qquad (3)$$

$$(\lambda - 1 \simeq \epsilon)$$

and shows a considerable dependence in (p,q), that is, in the molecular weight of the segment p,q. We are inclined to believe that mechanism A holds true at the onset of all deformations.[4] As t_1 (and consequently λ) increase, fewer cross links are effective and model B, for which there remains only cross links at both ends of the coil, is likely to be a better representation of the coil deformation. We shall interpret our data with a closed form model described in section II, which averages the effects of A and a special form of B, for which $p = 1$, $q = N$. It would be preferable to construct a model which interpolates between a maximum density of cross links along the coil (uniform affine deformation) and a minimum density (nonaffine coil deformation), but we have not yet found a simple interpolation formula.

(II) Neutron Scattering by Tagged Samples

The advantage of using nuclear rather than electromagnetic interaction in a scattering experiment has been reported earlier.[2a] Neutron scattering experiments by deuterated coils dispersed in a nonoriented protonated matrix have brought new information in coil statistics. For the problem of uniaxially stretched samples discussed in section I, much is to be gained by the knowledge of the scattering law

$$S_1(\mathbf{q}) = N^{-2} \sum_{i,j}^{N} \langle e^{i\mathbf{q}\cdot\mathbf{r}_{ij}} \rangle \qquad (4)$$

of the coil imbedded in the deformed bulk material (q is the momentum transfer, equal to $(4\pi/\mu) \sin \theta/2$, where μ is the neutron wavelength and θ is the scattering angle). A neutron small-angle scattering experiment was therefore made and scattered intensities I by the tagged samples of section I were recorded. The determination of $S_1(q)$ from the data is straightforward when the matrix in which the deuterated coils are dispersed does not scatter coherently by itself. The scattering law $S_1(q)$ is then simply the scattered intensity from the tagged sample, from which the intensity scattered by an untagged matrix is subtracted. The result is obtained in the form of

$$I(\mathbf{q}) = a + bS_1(\mathbf{q}) \qquad (5)$$

where a is the residual contribution of *incoherent* scattering and b is the intensity factor.

The underlying assumption is valid when the matrix is isotropic bulk material. In the case of a stretched film, there are, however, sources of coherent scattering by the matrix itself which may appear because of alignments of coils and appearance of voids and cracks. In such situations it is preferable to subtract from the intensity scattered by tagged stretched samples the intensity scattered by identically stretched untagged samples. (Even this procedure does not necessarily[7] provide the "null matrix" condition.) However, we have not used such procedures. Instead, we have simply subtracted the signal of an untagged unstretched sample from the intensity scattered by the mixed deuterated and protonated coils.

The experiment is conducted in such a way that the scattered intensity is measured for all orientations of the scattering vector q in the plane of the polystyrene films. The analysis of $S_1(\mathbf{q})$ for oriented material was discussed earlier[7] and since that time new aspects have been introduced.[8] In the first cumulant approximation, we can write the scattering law eq 4 as

$$S_1(\mathbf{q}) \simeq \frac{1}{N^2} \sum_{ij} \exp(-q^2 \langle R_{ij}^2(\hat{q})/2 \rangle) \qquad (6)$$

where $\langle R_{ij}^2(\hat{q}) \rangle$ is the average *squared* projection of $\mathbf{R}_{ij}$ on $\hat{q} = \mathbf{q}/|\mathbf{q}|$. Quite generally (6) may be written in terms of the radius of gyration R_{GO} of the unstretched coil

$$S_1(\mathbf{q}) = 2 \int_0^1 du(1-u) \exp(-q^2 R_{GO}^2 f_\lambda(u,\hat{q})) \qquad (7)$$

and of the approximate scaling law $f_\lambda(u,\hat{q})$, where $u = |i - j|/N$, for the stretched sample. We assume, according to ref 6 and 10, this law to be a combination of models A and B, i.e.,

$$f_\lambda(u,\hat{q}) = \lambda_A^2 u + (\lambda_B^2 - 1)u^2 \qquad (8)$$

for $\hat{q}$ in the stretch direction (q'') and

$$f(u,\hat{q}) = \lambda_A^{-1} u \qquad (9)$$

for q perpendicular to the stretch direction ($q^\perp$). The coefficients λ_A and λ_B are respectively the microscopic affine (model A) and nonaffine (model B) draw ratios. In the Guinier range of scattering vectors

$$S_1(q^\parallel) = 1 - q^{\parallel 2} R_{GO}^2 (\lambda_A^2 + (\lambda_B^2 - 1)/2)/3$$
$$= 1 - q^{\parallel 2} R^{\parallel 2}/3 \qquad (qR^\parallel < 1) \qquad (10)$$

$$S_1(q^\perp) = 1 - q^{\perp 2} R_{GO}^2 \lambda_A^{-1}/3$$
$$= 1 - q^{\perp 2} R^{\perp 2}/3 \qquad (qR^\perp < 1) \qquad (11)$$

In the transverse intermediate range $R^{\perp -1} < q < l^{-1}$, where l is the step length

$$S_1(q^\perp) = 2/(q^2 R^{\perp 2} + 1) \qquad (12)$$

For the longitudinal intermediate range $R^{\perp -1} < q < l^{-1}$, the scattering law eq 7 and 8 can be calculated in a closed eq 11 form as a function of $q^{\parallel 2}$ and the parameters λ_A, λ_B. Values $\lambda_B > 1$ indicate a rodlike behavior for small values of reciprocal

Table I

	Neutron wavelength, μm	Sample detector distance, m	Range of $\|\mathbf{q}\|$, Å^{-1}	Type of detector
Saclay	4.69 ± 0.04 Å $\Delta\mu/\mu$ = 0.75%		2×10^{-2} to 2×10^{-1} "intermediate range"	Two-axis simple counter
ILL	8.3 Å $\Delta\mu/\mu$ = 50%[a]	20	2.5×10^{-3} to 1.2×10^{-2} "Guinier range"	Two-dimensional x,y detector
	6 Å $\Delta\mu/\mu$ = 8%	5	1.2×10^{-2} to 6×10^{-1} "intermediate range"	

[a] Corrections have been made on the measured intensities according to ref 1 to eliminate the wavelength dispersion effects.

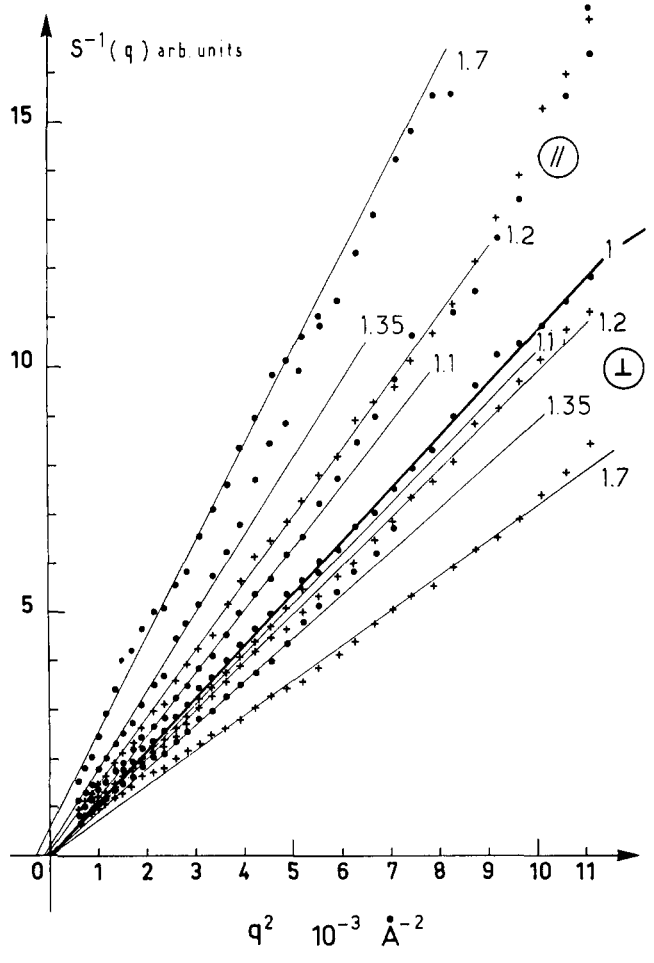

Figure 2. Inverse scattered intensities in the intermediate momentum range $3 \times 10^{-2} < q < 10^{-1}$ Å^{-1} along $q_x(S^{\parallel})$ and $q_y(S^{\perp})$. The values of λ are reported on the diagram.

space $q^{\parallel}$ (high distances in real space) and random coil like behavior for higher values of reciprocal space $q^{\parallel}$ (smaller distances in real space). The crossover occurs at

$$q^{\parallel *} = (\lambda_B{}^2 - 1)^{1/2}/2^{1/2}\lambda_A R_{GO} \quad (13)$$

which measures the relative importances of the effects of mechanism B to mechanism A. For $q^{\parallel} > q^{\parallel *}$, the scattering law $S_1(q^{\parallel})$ was shown in ref 5 to tend asymptotically to the form

$$S_1(q^{\parallel}) = 2/(q^{\parallel 2}R_{GO}{}^2\lambda_A{}^2 + 1 + \kappa^2 R_{GO}{}^2\lambda_A{}^2) \quad (14)$$
$$(q^{\parallel} > q^{\parallel *})$$

where $\kappa = 6^{1/2}(\lambda_B{}^2 - 1)^{1/2}R_{GO}{}^{-1}$. *For* $q^{\parallel} < q^{\parallel *}$, $S_1(q^{\parallel})$ has a rodlike behavior, i.e., $\sim q^{\parallel -1}$. It is important to notice that the transverse dimensions and correlations are not affected by mechanism B.

The particular case $\lambda_A = 1$ and $\lambda_B = 1$ leads of course to the Debye formulation of $S_1(q)$, which was shown in ref 1 to interpret satisfactorily the data on unstretched tagged samples.

(III) Data Analysis

The scattering experiments were made both in Saclay (EL III) and in Grenoble (ILL), using the neutron cold source, the neutron guide, and the detector which are described in more detail in ref 2a and 9. Two characteristic momentum transfer ranges were investigated, the small angle Guinier range ($q < R_{GO}{}^{-1}$) and the small angle intermediate range ($R_{GO}{}^{-1} < q < l^{-1}$). Two sets of samples were tested, for small elongations ($\lambda \leq 1.7$) and for higher elongations ($\lambda > 2$), respectively. The experimental conditions are summarized in Table I.

Because our main result is obtained in the intermediate range, we shall first report and discuss the data concerning this range.

(1) Scattered Intensities in the Intermediate Range. (a) Small Elongation Samples. For these samples the temperature T_1 is 120 °C. The inverse scattering laws $S_1{}^{-1}(q)$ are shown in Figure 2 as a function of $q^{\perp 2}$ (transverse direction) and $q^{\parallel 2}$ (longitudinal direction) for several values of $\lambda \leq 1.7$. There is no marked deviation from the linear (Debye) dependence in $q^{\perp 2}$ and $q^{\parallel 2}$. The slopes of $(S^{\perp})^{-1}$ decrease with λ, those of $(S^{\parallel})^{-1}$ increase with λ. These are characteristics of mechanism A. More precisely, if we consider the products $R_i{}^{\parallel}R_i{}^{\perp 2}/R_{GO}{}^3$ where $R_i{}^{\parallel 2}$ and $R_i{}^{\perp 2}$ are respectively the slopes of $S^{\parallel -1}$ vs. $q^{\parallel 2}$ and $S^{\perp -1}$ vs. $q^{\perp 2}$, we notice in Table II that they are not strictly constant as a function of λ.

In fact they decrease slightly as λ increases. Also, as λ becomes equal to 1.7, the intercept κ of $S^{\parallel -1}$ with the q^2 axis is seen in Figure 2 to be nonzero. In terms of λ_B (eq 4) we have $\lambda_B = 1.3$. According to ref 5, a finite value of κ is determined by a finite value of the average orientation $\langle \cos \omega \rangle$, which in this case is about 0.1. These facts indicate that, although mechanism A is dominant at small elongations, one cannot completely eliminate the presence of mechanism B.

(b) Higher Elongation Samples. These samples have been drawn at a constant velocity gradient $s = 0.18$ s^{-1} and the extension ratios λ were measured from lines marked on the sample in the vicinity of the neutron scattering area.

Thickness and neutron transmission of the samples are reported in Table III.

Inverse scattering laws are shown in Figure 3 for $\lambda = 3$ at two temperatures T_1, respectively 110 and 130 °C. The scattering laws in Figure 4 correspond to $\lambda = 4.5$ and $T_1 = 120$ °C, with a partial recovery $\tilde{L} = 0.95L$ for one sample (Re) and no recovery for the other.

The main difference with respect to the previous case (Figure 2) is the deviation of $S^{\parallel -1}$ from the linear behavior in q^2, for a squared momentum range in which the transverse

Table II
Characteristic Data Obtained from the Scattering Experiments by the Small-Elongation Samples

Extension ratio λ	$R_i^{\parallel}R_i^{\perp 2}/R_{GO}^3$	$R^{\parallel}$, Å	$R^{\perp}$, Å	$R^{\parallel}R^{\perp 2}/R_{GO}^3$	$R^{\parallel}/R_i^{\parallel}$	$R^{\perp}/R_i^{\perp}$
1	1	86.5	86	1		
1.1	1.05	90.5	83.5	0.97	0.62	0.7
1.22	1.05	91.5	80.5	0.91	0.58	0.69
1.35	0.95	95.5	78.5	0.90	0.57	0.7
1.57		106.5	73.5	0.89		
1.7	0.95	128	68	0.91	0.8	0.69

Table III
Neutron Transmissions of the High-Extension Samples

Sample	Purely protonated polystyrene	1% deuterated			
		$\lambda = 1$	$\lambda = 3$, $T_1 = 110$ °C	$\lambda = 3$, $T_1 = 130$ °C	$\lambda = 4.5$, $T_1 = 120$ °C
Tickness t, mm	0.97	0.93	1.19	1.4	0.97
Neutron transmission	0.669	0.686	0.662	0.638	0.70
Intensity I	889				
scattered at $q = 1$ Å^{-1} in arbitrary units	889	851	986	1090	772
I/t arbitrary units	1.36	1.33	1.25	1.22	1.13

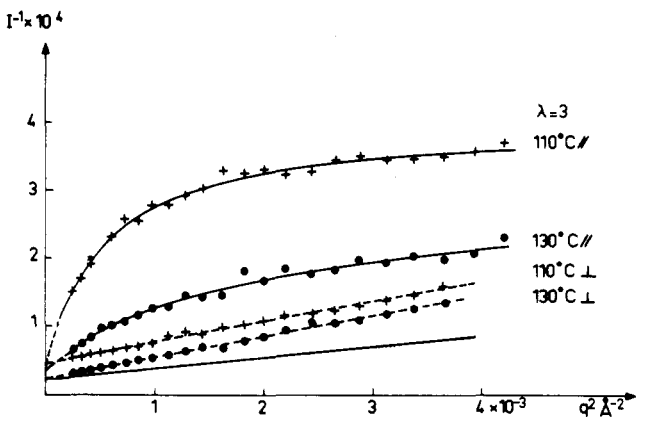

Figure 3. Inverse scattering intensities for two temperatures T_1 in the intermediate momentum range $1.1 \times 10^{-2} \leq q \leq 10^{-1}$ along $q_x^2(S^{\parallel})$ and $q_y^2(S^{\perp})$. Draw ratio $\lambda = 3$. The dots and circles are measured values. The continuous lines are calculated scattered intensities according to (5), (7), and (8) in the longitudinal direction. The broken lines are linear interpolations of the transverse data. The experimental points are normalized according to the procedure described in ref 1. The continuous straight line is the transverse inverse scattering law for $T_1 = 110$ °C normalized to the data of $T_1 = 130$ °C according to eq 11.

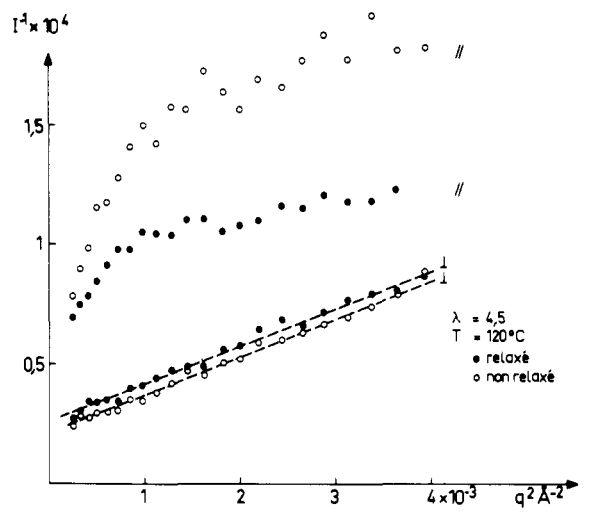

Figure 4. Inverse scattered intensities as in Figure 3. Draw ratio $\lambda = 4.5$. Hot stretch temperature $T_1 = 120$ °C. The two sets of curves illustrate the effect of partial recovery between stretch and quench phases: (○) without partial recovery; (●) with partial recovery.

correlations $S^{\perp -1}$ are strictly linear.

This range extends from 3.6×10^{-4} Å^{-2} to 4×10^{-3} Å^{-2}, as compared respectively to 6.6×10^{-4} Å^{-2} and 1.1×10^{-2} Å^{-2} in Figure 2. Equations 5, 7, and 8 were fitted to the data of Figure 3 observed in the longitudinal direction, with the optimization procedure described in ref 12. The best fit values of the parameters are given in Table IV. The results are essentially the temperature dependences of λ_A and λ_B. Thus at $T_1 = 110$ °C, λ_A is greater than λ_B, and the deformation is essentially affine. For a higher temperature $T_1 = 130$ °C, the longitudinal deformation of the coil is still as important as in the case of the deformation nearer to the glass temperature T_G, but λ_A is smaller than λ_B. It is nonaffine in the sense of mechanism B, which means that the chain is deformed by end-to-end stretching. All this is summarized in the fact that q^* as defined in eq 13 increases with T_1.

If we recall the relations between segment orientation and extension ratio (eq 2)

$$\lambda_A \simeq \tfrac{1}{6} + \tfrac{5}{2}\langle\cos^2\omega\rangle \qquad (\lambda_A - 1 \sim \epsilon)$$

and (eq 14)

$$\lambda_B \simeq 1 + 3N(\langle\cos\omega\rangle)^2 \qquad (\lambda_B - 1 \sim \epsilon)$$

then the result of Figure 3 can be described as follows.

(1) The disorientation of the segments (i.e., the proximity of $\langle\cos^2\omega\rangle$ to the random orientation value $\frac{1}{3}$) increases with T_1. This is the well-known result observed from birefringence experiments[2b] but could not easily be understood since, whatever the disorientation, there is full recovery of the initial sample length when the sample is heated above T_1 after the quench phase.

(2) A plausible interpretation is now given by the observation of $\langle\cos\omega\rangle$. This average cannot be observed by optical

Table IV
Characteristic Values of the Microscopic Elongation Ratios Obtained from the Interpretation of Figure 3 with Equations 5, 7, and 8

λ	T_1 °C	R_{GO}	a	b	λ_A	λ_B	q^*	$(\lambda_A{}^2(\lambda_B{}^2 - 1)/2)^{1/2}$
3	110	86 Å	$2.5 \times 10^{-2} \pm 10^{-4}$	0.3 ± 0.1	2.52 ± 0.1	1.15 ± 0.1	$5 \times 10^{-3} \pm 1 \times 10^{-3}$	$6.45^{1/2}$
3	130	86 Å	$2.5 \times 10^{-2} \pm 10^{-4}$	0.3 ± 0.4	0.81 ± 0.3	3.1 ± 4	$3.4 \times 10^{-2} \pm 1 \times 10^{-2}$	$4.89^{1/2}$

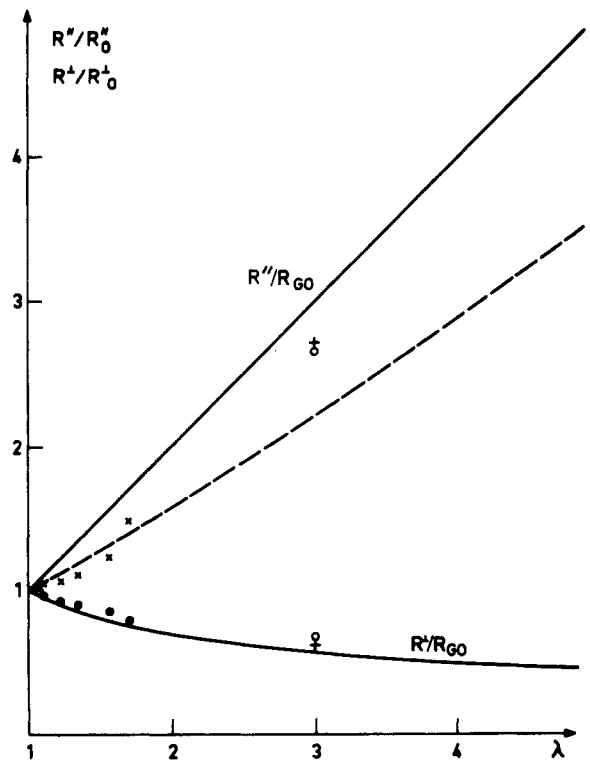

Figure 5. Radii measured in the longitudinal and transverse direction as a function of λ. The continuous lines correspond to the purely affine deformation ($\lambda = \lambda_A$). The broken line corresponds to the nonaffine deformation model ($\lambda = \lambda_B$).

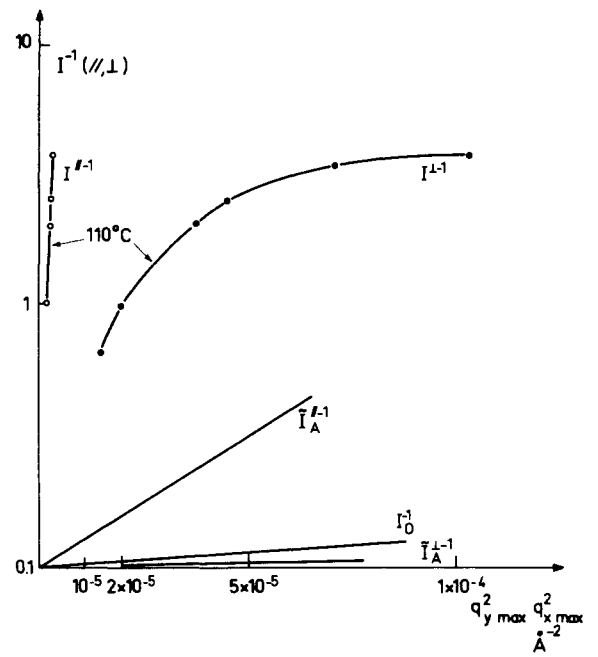

Figure 6. Guinier plot of the inverse scattering law for the sample $\lambda = 3$, $T_1 = 110$ °C. For comparison, the straigth lines obtained with a hypothetical coil affinely deformed are given in the lower part of the figure (I_a).

methods and its determination is a characteristic result of the neutron scattering technique. The $q^{\parallel}$ dependence of S_1 indicates that λ_B, therefore[5] $\langle \cos \omega \rangle$, increases with T_1. Thus while $\langle \cos \omega^2 \rangle$ tends toward $\frac{1}{3}$ (which is called disorientation), the coil elongation is maintained by the increase of the average value $\langle \cos \omega \rangle$.

It was shown in section II that the model function $S_1(q^{\parallel})$ could be seen as succession of a rodlike behavior at large distances (or small values of reciprocal space $q^{\parallel} < q^{\parallel *}$) and a coillike behavior at smaller distances (or larger values of reciprocal space $q > 1^*$). The longitudinal data indicate that the range of reciprocal space in which the coil can be seen as a rod is greater at $T_1 = 130$ °C than at $T_1 = 110$ °C.

The transverse correlations $S_1{}^{\perp -1}$ in Figure 3 are interpolated from the observed data as a linear function of $q^{\perp 2}$. The abscissa of the extrapolation to $S_1{}^{\perp -1} = 0$ is seen to decrease with temperature, which indicates according to eq 12 that the contribution of mechanism A to the deformation decreases with T_1 as noted in the longitudinal case. The values obtained for λ_A in the transverse case are however found to be twice as great as in Table IV.

Consistency between transverse and longitudinal interpolated parameters of eq 5, 7, and 8 is not satisfactory. Especially, the normalization constants b which are found to be identically the same in the longitudinal and transverse functions for $T_1 = 130$ °C differ by a factor 2 for $T_1 = 110$ °C. This indicates a failure in the model to interpret correctly the data. A possible improvement consists in replacing the interpolation between the two extreme cases of a maximum and a minimum density of effective crosslinks along the chain (respectively models A and B) by a model function which includes all intermediate cases.

The partial recovery experiment (Figure 4) shows an interesting difference with respect to Figure 3. The transverse correlations are hardly affected by the recovery, which indicates in terms of A and B that the contribution of A to the coil deformation has not changed. Thus the considerable change observed on the longitudinal correlations only reflects decrease of λ_B. The material recovers by decrease of the end-to-end distances, rather than by disorientation of the segments.

(2) Scattered Intensity in the Guinier Range. (a) Small Elongation Samples. The Zimm plot analysis along $q^{\parallel 2}$ and $q^{\perp 2}$ gives the radii reported in Table II and drawn on Figure 5. The affine deformation radii derived from eq 10 and 11 for $\lambda_A = \lambda$ are also drawn in this figure. The discrepancy probably reflects the fact that the indicated draw ratio λ was measured from the film end-to-end distance, which is somewhat greater than the draw ratio in the scattering area because of end effects.

The ratios $R^{\parallel}R^{\perp 2}/R_{GO}{}^3$ decrease slightly as λ increases. The ratios $R^{\parallel}/R_i{}^{\parallel}$ are seen to be constant. As in the previous section, it is concluded that the deformation on the radius of gyration scale is essentially affine with a small contribution of mechanism B as $\lambda = 1.7$.

(b) High-Elongation Sample. The Guinier plot of the

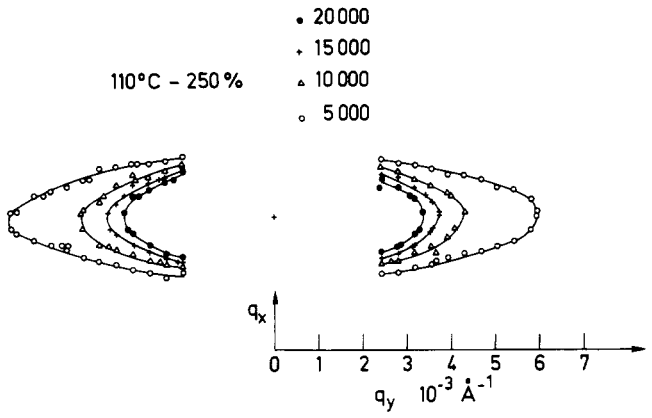

Figure 7. Lines of constant scattered intensities in the q_x, q_y plane. Draw ratio $\lambda = 3$, $T_1 = 110$ °C. The area $A = 5 \times 5 \times 10^{-6}$ Å^{-2} centered at the origin of the ellipses is the cross section of the direct beam (the origin of the q_x, q_y system is the center of the ellipses).

scattered intensities for the sample $\lambda = 3$, $T_1 = 110$ °C is shown in Figure 2. In contradistinction to the smaller elongations, the data show a nonlinear behavior in $q^{\parallel 2}$ and $q^{\perp 2}$ of the scattered intensity in this representation. Thus we cannot measure a radius of gyration. This behavior can be explained by the presence of voids or cracks which appear as the material is stretched. As $q^{\parallel}$ reaches the value 10^{-1} Å^{-1} in Figure 6, a slope emerges from the graph, which is comparable to what a purely affine deformed coil would give.

Lines of constant scattered intensities in the q_x, q_y plane are shown in Figure 7. These lines have been fitted to ellipses. The ellipticity (ratio of great axis to small axis minus one) is found to be $e = 4.1$, for $q^{\perp} = 10^{-2}$ Å^{-1}. The draw ratio associated to these ellipses in the hypothesis of a purely affine deformation is $\lambda = (e + 1)^{2/3} = 2.9$. This value is reported in Figure 7.

(IV) Conclusion

Our main result is the observation of the coil asymptotic scattering law in the intermediate momentum range in relation to draw ratio, hot stretch temperature, and partial recovery. At the onset of the uniaxial stretching, the inverse scattering laws are linear in q^2, both in the transverse and in the longitudinal direction. For higher elongations ($\lambda \geq 2$), this function is still perfectly linear in q^2 in the transverse direction, whereas it shows a distinct curvature in the longitudinal direction. The curvature is particularly noticeable for the smaller values q of the intermediate momentum range. The shape of this function is extremely sensitive upon the values of λ, T_1, and partial recovery. The slopes of the inverse scattering law in the transverse direction decrease with λ and increase with T_1.

A model was fitted to the observed longitudinal data which combines affine and nonaffine deformation of the coil. The temperatures show that:

(1) For a given draw ratio ($\lambda = 3$), the contribution of the purely affine mechanism to the coil deformation decreases with temperature. This means that the molecular orientation decreases, in the sense that the average squared segment orientation $\langle \cos^2 \omega \rangle$ tends to its random value ⅓. This result was already known from birefringence experiments.

(2) The contribution of the nonaffine mechanism increases with temperature. The scattering law dependence on momentum transfer q shows how the loss of this segment orientation is compensated by a long-range correlation implying a finite value of $\langle \cos \omega \rangle$. This is new information provided by the neutron scattering experiments.

These mechanisms are perhaps not the most appropriate ones for the description of such viscoelastic deformations. A better starting point would be the evaluation of a reciprocal space size q^* below which the deformation is affine and above which the deformation is no more affine.[4] Such a calculation is given in the Appendix for a particular situation.

Acknowledgments. We are very thankful to C. Bonnebat, T. Alfrey, P. G. de Gennes, S. Daoudi, R. Ghosh, M. Tournarie, and J. des Cloizeaux for helpful advice and comments. One of us (G. J.) wishes to thank the Department of Nuclear Engineering (Ann Arbor, Mich.) for a visit during which these problems were discussed.

Appendix. Neutron Elastic Scattering from a Rouse Chain in a Longitudinal Velocity Gradient

In this section we study the internal conformations of an isolated flexible polymer in the presence of a longitudinal velocity gradient of the solvent. In order to attempt to make some contact with the situation of polymer melt which is the subject of this experimental investigation, we neglect both excluded volume and hydrodynamic interactions which are strongly screened out in concentrated systems.[6] The equation of motion for the nth monomer at position $\mathbf{r}_n$ is written.

$$\dot{\mathbf{r}}_n = \mathbf{v}(\mathbf{r}_n) + B\phi_n \tag{A.1}$$

where $\mathbf{v}(\mathbf{r}_n)$ is the velocity field at the nth monomer which we take to be

$$\mathbf{v}(\mathbf{r}_n) = s x_n \hat{u} \tag{A.2}$$

where s is the velocity gradient which is longitudinal along the x direction. The second term represents the response to the total force ϕ_n experienced by the nth monomer, where B is the microscopic monomer mobility which in principle should be self-consistently determined in a melt. We shall assume it here to be constant.

For weak deformations, the force ϕ_n may be taken to be simply the entropic Hookean term

$$\phi_n = (\zeta k_B T/a^2)(\mathbf{a}_n - \mathbf{a}_{n-1}) \tag{A.3}$$

with

$$\mathbf{a}_n = \mathbf{r}_{n+1} - \mathbf{r}_n \tag{A.4}$$

The drift term may be combined with elastic force to give an effective total force $\tilde{\phi}_n$,

$$\tilde{\phi}_n = \phi_n + (s/B) x_n \hat{1} \tag{A.5}$$

which may be derived from the potential energy

$$V = (3k_B T/2a^2) \sum_n (a_n{}^2 - \sigma x_n{}^2) \tag{A.6}$$

with $\sigma = sa^2/3k_B TB = s\tau/3N^2$, where $\tau^{-1} = BT/(Na)^2$ is the Ronse relaxation time (roughly the time for the coil to diffuse one diameter). In the continuum approximation $\mathbf{a}_n = \partial \mathbf{r}_n/\partial_n$, and assuming free ends $a_0 = a_n = 0$, we "Fourier" transform the potential energy to obtain

$$V = (3Nk_B T/4a^2) \sum_k (k^2 r_k{}^2 - \sigma x_k{}^2) \tag{A.7}$$

where

$$\mathbf{r}_n = \sum_k \mathbf{r}_k \cos kn \tag{A.8}$$

and $k = p\pi/N$, $p = 1, 2, \ldots, N$. The equipartition theorem immediately gives the thermodynamic averages of the Fourier amplitudes

$$\mathbf{r}_k = 0$$

$$\langle y_k{}^2 \rangle = \langle Z_k{}^2 \rangle = 2a^2/3Nk^2$$

$$\langle x_k^2 \rangle = \langle 2a^2/3N \rangle (k^2 - \sigma)^{-1} \quad \text{(A.9)}$$

In this linear regime, the transverse dimensions are essentially unmodified, while the longitudinal response exhibits a divergence when $s_c\tau \simeq 3\pi^2$. This is the "coil stretch" transition discussed in more detail by de Gennes.[13] When $s \geq s_c$, we must include nonlinear elastic terms. Restricting our attention to the linear regime $s \lesssim s_c$, the Fourier intensities (A.9) may be used to compute conformational properties. For example, the mean-square end-to-end component along the velocity gradient is

$$\langle (x_N - x_0)^2 \rangle = 4 \sum_{p \atop (\text{odd})} \langle x_p^2 \rangle \equiv \left(\frac{8a^2}{3N}\right) \sum_{p \atop (\text{odd})} (k^2 - \sigma)^{-1}$$
$$\simeq (8/3\pi^2) N a^2 (1 - s/s_c)^{-1} \quad \text{(A.10)}$$

This result implies that in the presence of a longitudinal gradient, the coil becomes ellipsoidal with the major axis parallel to the velocity gradient. In the neighborhood of s_c the system jumps to a new strongly stretched state.[13,14]

The neutron scattering structure factor is given by

$$S_1(\mathbf{q}) = \sum_{ij} \langle e^{i\mathbf{q}\cdot(\mathbf{r}_i - \mathbf{r}_j)} \rangle \quad \text{(A.11)}$$

which for stochastic coils may be approximated as

$$S_1(\mathbf{q}) = \sum_{ij} e^{-1/2(q^2)\langle (b_i - b_j)^2 \rangle} \quad \text{(A.12)}$$

where b_i is the component of $\mathbf{r}_i$ along $\mathbf{q}$. For the scattering vector perpendicular to the velocity gradient we therefore find the familiar Debye q^{-2} law which may be demonstrated as follows. The average square separation between two monomers (say the y direction) is

$$\langle (y_i - y_j)^2 \rangle = (2a^3/3N) \sum_k k^{-2} (\cos ki - \cos kj)^2 \quad \text{(A.13)}$$

$$\langle (y_i - y_j)^2 \rangle$$
$$= (2a^2/3N) \sum_k k^{-2} [\cos ki (1 - \cos k\Delta) - \sin ki \sin k\Delta]^2$$

where $\Delta = |i - j|$. In order to simplify the calculation and eliminate end effects, we average over i to give (for $\Delta/N \ll 1$)

$$\langle (y_i - y_j)^2 \rangle = (4a^2/3N) \sum_k k^{-2} \sin^2 \frac{k\Delta}{2} = \tfrac{1}{3} a^2 \Delta \quad \text{(A.14)}$$

which when substituted into (A.12) gives $S^T(q) = 12/a^2q^2$, the usual Debye law for the intermediate range.

Along the direction of the velocity gradient

$$\langle (x_i - x_j)^2 \rangle$$
$$\cong \tfrac{1}{3} a^2 \Delta + \frac{a^2 \Delta^2}{6N} (s/s_c)^{1/2} \ln \left(\frac{1 + (s/s_c)^{1/2}}{1 - (s/s_c)^{1/2}}\right) \quad \text{(A.15)}$$

This is of the form of a stretched chain (cf. eq 8)

$$\langle (x_i - x_j)^2 \rangle \simeq \tfrac{1}{3} a^2 \Delta + \Delta^2 \bar{a}^2 = \frac{N}{3} a^2 u + N^2 \bar{a}^2 u^2 \quad \text{(A.16)}$$

where $\bar{a}$ is the mean monomer separation. There is then a transition between the Debye regime at short wavelength and a rigid rod behavior ($S \sim q^{-1}$) at long wavelengths with the crossover occurring at q^* ($q^*a \sim \bar{a}/a$), which for our case is

$$(q^* R_0)^2 \simeq \tfrac{1}{6} (s/s_c)^{1/2} \ln \left(\frac{1 + (s/s_c)^{1/2}}{1 - (s/s_c)^{1/2}}\right) \quad \text{(A.17)}$$

Thus the rigid rodlike intermediate regime occurs only for gradients in the vicinity of s_c.

References and Notes

(1) (a) C. R. M.; (b) Laboratory Léon Brillouin; (c) Centre de Recherche de la Croix de Berny; (d) Collège de France.
(2) (a) J. P. Cotton, D. Decker, H. Benoit, B. Farnoux, C. Picot, G. Jannink, R. Ober, and J. des Cloizeaux, *Macromolecules*, **7**, 864 (1974); (b) K. J. Cleereman, H. J. Karam, and J. L. Williams, "Modern Plastic", Breskin Publications Inc., New York, N.Y., 1953.
(3) A. J. de Vries, C. Bonnebat, and J. Beautemps, presented at the I.U.P.A.C. Conference, Budapest, 1976.
(4) S. Daoudi and P. G. de Gennes, to be published. See also S. F. Edwards, *Proc. Phys. Soc., London*, **92**, 9 (1967).
(5) H. Benoit, R. Duplessix, R. Ober, M. Daoud, J. P. Cotton, B. Farnoux, and G. Jannink, *Macromolecules*, **8**, 451 (1975).
(6) R. J. Roe and W. R. Krigbaum, *J. Appl. Phys.*, **35**, 2215 (1964).
(7) J. S. King, G. Summerfield, and R. Ullman, to be published.
(8) P. G. de Gennes, P. Pincus, R. M. Velasco, and F. Brochard, to appear in *J. Phys. (Paris)*.
(9) Neutron Beam Facilities, ILL, BP 156 Centre de tri 38042 Grenoble.
(10) W. Kuhn, O. Kunzle, and A. Katchalsky, *Helv. Chim. Acta*, **31**, 1994 (1948).
(11) R. K. Bullough, *Physica*, **29**, 433 (1963).
(12) M. Tournarie, *J. Phys. (Paris)*, **10**, 737 (1969).
(13) P. G. de Gennes, *J. Chem. Phys.*, **60**, 5030 (1974).
(14) S. Daoudi, *J. Phys. (Paris)*, **10**, 737 (1969).